© 2021. Published by The Company of Biologists Ltd | Journal of Cell Science (2021) 134, jcs258446. doi:10.1242/jcs.258446

RESEARCH ARTICLE

Enrichment of Z_α domains at cytoplasmic stress granules is due to their innate ability to bind to nucleic acids

Luisa Gabriel[§], Bharath Srinivasan[*,§,], Krzysztof Kuś[‡,§], João F. Mata, Maria João Amorim, Lars E. T. Jansen[‡] and Alekos Athanasiadis[¶]**

ABSTRACT

Z_α domains recognize the left-handed helical Z conformation of double-stranded nucleic acids. They are found in proteins involved in the nucleic acid sensory pathway of the vertebrate innate immune system and host evasion by viral pathogens. Previously, it has been demonstrated that ADAR1 (encoded by *ADAR* in humans) and DAI (also known as ZBP1) localize to cytoplasmic stress granules (SGs), and this localization is mediated by their Z_α domains. To investigate the mechanism, we determined the interactions and localization pattern for the N-terminal region of human DAI ($Z_{\alpha\beta}^{DAI}$), which harbours two Z_α domains, and for a $Z_{\alpha\beta}^{DAI}$ mutant deficient in nucleic acid binding. Electrophoretic mobility shift assays demonstrated the ability of $Z_{\alpha\beta}^{DAI}$ to bind to hyperedited nucleic acids, which are enriched in SGs. Furthermore, using immunofluorescence and immunoprecipitation coupled with mass spectrometry, we identified several interacting partners of the $Z_{\alpha\beta}^{DAI}$–RNA complex *in vivo* under conditions of arsenite-induced stress. These interactions are lost upon loss of nucleic acid-binding ability or upon RNase treatment. Thus, we posit that the mechanism for the translocation of Z_α domain-containing proteins to SGs is mainly mediated by the nucleic acid-binding ability of their Z_α domains.

This article has an associated First Person interview with Bharath Srinivasan, joint first author of the paper.

KEY WORDS: ADAR1, $Z_{\alpha\beta}^{DAI}$ domain, Z-DNA, Stress granules, RNA-binding proteins, DAI

INTRODUCTION

Z_α domains belong to an unusual nucleic acid-binding domain family that recognizes purine-pyrimidine repeats (Kim et al., 2004; Oh et al., 2002) in the left-handed Z conformation of both DNA and RNA helices (Placido et al., 2007; Schwartz et al., 1999), both *in vitro* and *in vivo*. The prototypic Z_α domain was identified as part of the large isoform of ADAR1 (encoded by *ADAR* in humans), an interferon (IFN)-inducible RNA-editing enzyme, and all subsequently identified Z_α domains have been shown to be components of IFN-inducible proteins or viral inhibitors of the IFN pathway (Athanasiadis, 2012) (Fig. 1A). ADAR1 is known to be a negative regulator of the double-stranded RNA (dsRNA)-sensing pathway and has an important role in preventing activation of the pathway by self RNAs. Mutations in ADAR1, some within the Z_α domain, have been implicated in causing Aicardi–Goutières syndrome, an auto-inflammatory genetic disease (Rice et al., 2012). Two other cellular proteins that have Z_α domains are DAI (also known as ZBP1) and PKZ (Fig. 1A). DAI is a mammalian sensor of dsDNA (Takaoka et al., 2007), whereas PKZ is a fish-specific effector of dsRNA recognition, having a role analogous to PKR (also known as EIF2AK2; Rothenburg et al., 2005). Two more proteins containing Z_α domains are both encoded by DNA viruses: E3L from poxviruses (Kim et al., 2003) and ORF112, a protein we recently described in a subfamily of herpesviruses (Kuś et al., 2015) (Fig. 1A). Both viral proteins have a role in innate immune evasion and are required for viral proliferation. In the case of E3L, it has been shown that deletion of the E3L Z_α domain causes loss of virus pathogenicity, and replacement of the domain with Z_α domains from either ADAR1 or DAI fully restores pathogenicity (Kim et al., 2003), suggesting that Z_α domains from different proteins have similar function.

Although the degree of conservation among Z_α domains is moderate, key DNA- and RNA-interacting residues, identified in crystal structures of Z_α–DNA and Z_α–RNA complexes (Placido et al., 2007; Schwartz et al., 1999), are absolutely conserved and thus provide a motif for the unambiguous identification of the domains, which otherwise demonstrate the common winged helix-turn-helix (wHTH) fold (Athanasiadis, 2012) (Fig. 1B,C). Studies of Z_α domains have primarily focused on the mechanism of their interaction with DNA and RNA that has adopted the left-handed Z conformation (Z-DNA and Z-RNA, respectively), mostly through structural and biochemical studies (De Rosa et al., 2010; De Rosa et al., 2013; Kim et al., 2011; Schwartz et al., 2001; Sung et al., 2008). Thus, although there are now structures of Z_α domains in complexes with nucleic acids from all known Z_α-containing proteins (De Rosa et al., 2013; Ha et al., 2004; Kuś et al., 2015; Schwartz et al., 1999; Schwartz et al., 2001), little is known regarding the *in vivo* targets and functions of the domains.

Z_α domains *in vitro* can bind to the double helix of both DNA and RNA, taking advantage of the fact that, unlike the common right-handed helices of the two macromolecules (the B- and A- forms, respectively), which have very different structures, their left-handed Z-form helix is very similar (Placido et al., 2007). Thus, the question whether Z_α domains target DNA or RNA *in vivo* is open. Nevertheless, the fact that proteins containing Z_α domains are predominantly cytoplasmic and have a function in the RNA-sensing pathway strongly points to a Z_α association with dsRNA and/or RNA–DNA hybrids. An affinity of Z_α domains for segments of ribosomal RNA (Feng et al., 2011) has been shown through analysis of RNA pulldowns in both *E. coli* and human cell extracts. The same

Instituto Gulbenkian de Ciência, Rua Quinta Grande 6, Oeiras 2781-156, Portugal. *Present address: Mechanistic Biology and Profiling, Discovery Sciences, R&D, AstraZeneca, Cambridge CB4 0WG, UK. ‡Present address: Department of Biochemistry, University of Oxford, South Parks Road, Oxford OX1 3QU, UK. §These authors contributed equally to this work ¶Deceased

**Author for correspondence (bharath.srinivasan@astrazeneca.com)

L.G., 0000-0001-9153-219X; B.S., 0000-0003-0561-213X; M.J.A., 0000-0002-4129-6659; L.E.T.J., 0000-0002-2158-0345; A.A., 0000-0003-1526-0000

Handling Editor: Maria Carmo-Fonseca
Received 21 January 2021; Accepted 8 April 2021

Journal of Cell Science (2021) 134, jcs258446. doi:10.1242/jcs.258446

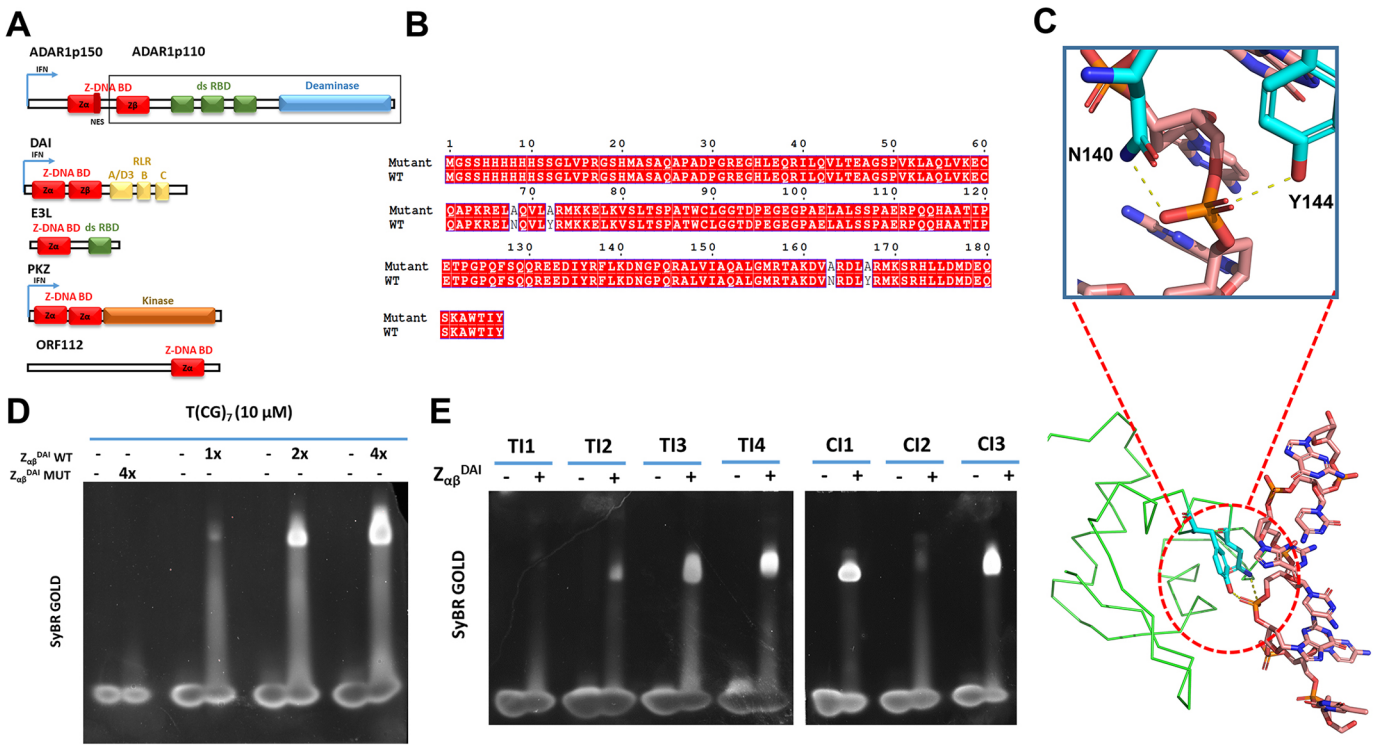

Fig. 1. Structural features and *in vitro* nucleic acid binding of Z_α domains (A) Domain organization of different human and viral proteins possessing the Z_α domain. ADAR1, adenosine deaminase acting on RNA 1 (p150 and p110 are ADAR1 isoforms of different lengths; the black box indicates the domain organization of the p110 isoform); DAI, DNA-dependent activator of IFN-regulatory factors; E3L, vaccinia virus protein that inhibits ZBP1-induced necroptosis via interaction with host ZBP1; PKZ, fish homologue of double-stranded RNA-dependent protein kinase (PKR); ORF112, RNA-binding protein from cyprinid herpesvirus. ds RBD, dsRNA-binding domain; IFN, interferon-inducible promoter; NES, nuclear export signal; RLR, RHIM-like repeat; RHIM, RIP homotypic interaction motif; Z-DNA BD, Z-DNA-binding domain. (B) Pairwise sequence alignment of the WT and mutant $Z_{\alpha\beta}^{DAI}$ domains indicating the residues that were mutated across the two Z_α domains (white). The alignment was generated using T-Coffee and the image was rendered with ESPript 3.0. Amino acid residues are numbered based on the construct shown in Table S7. (C) The structure shows a Z_α domain of DAI bound to the nucleic acid (PDB ID: 3eyi) highlighting the asparagine and tyrosine residues implicated in nucleic acid recognition. The protein chain is shown in ribbon representation, while the interacting residues from protein and the DNA are shown as ball and stick representation in cyan and brown, respectively. The hydrogen bonding interaction between the side-chain NH group of asparagine and the hydroxyl group of tyrosine with the backbone phosphates are shown as dotted lines. The figure was rendered using Open-Source PyMol (D) An EMSA to show the DNA binding by the WT protein ($Z_{\alpha\beta}^{DAI}$ WT) and the abolishment of DNA binding for the quadruple mutant with asparagine and tyrosine residues mutated in both the Z_α domains ($Z_{\alpha\beta}^{DAI}$ MUT). The WT protein binds to the DNA in a concentration-dependent manner (1×, 2× and 4× represent 10 µM, 20 µM and 40 µM of the protein, respectively). (E) An EMSA showing the interaction of the WT $Z_{\alpha\beta}^{DAI}$ with hyperedited nucleic acids, which are enriched in SGs. The TI series (TI1–TI4) are duplex oligonucleotides containing thymidine-inosine repeats (top strands: TI1, 5′-GGCCTITIGGCC-3′; TI2, 5′-CGCGTITICGCG-3′; TI3, 5′-CGCGTITITICGCG-3′; TI4, 5′-GGCCTITITIGGCC-3′), and the CI series (CI1–CI3) contains cytosine-inosine repeats (top strands: CI1, 5′-CGCGCICICGCG-3′; CI2, 5′-CCGGCICICCGG-3′; CI3, 5′-CGCGCICICICGCG-3′). Data in D and E are representative of three independent experiments.

study showed that that expression of Z_α domains can inhibit translation, although it is not clear if this inhibition is the result of binding to the suggested ribosomal RNA sites. In another work investigating the Z-DNA content of the genome, using Z_α domains as reporter, it was reported that Z_α can interact with centromeric repeats (Li et al., 2009). In both cases, the physiological relevance of the described interactions remains unexplored, and no clear link is established for the function of Z_α-containing proteins.

Two of the Z_α-containing proteins, ADAR1 and DAI, have been shown to associate with stress granules (SGs) (Deigendesch et al., 2006; Weissbach and Scadden, 2012). SGs are cytoplasmic RNPs containing stalled ribosomes, the result of stress-induced translation arrest. Challenging cells with arsenite results in reactive oxygen species production that, in turn, activates haem-regulated inhibitor kinase (HRI, also known as EIF2AK1). HRI phosphorylates eIF2α (EIF2A) preventing turnover of the ternary $tRNAi^{Met}$–GTP-eIF2 complex. This results in stalled translation initiation complexes that are assembled into discrete cytoplasmic foci known as SGs (Lu et al., 2001). It has been shown that hyperedited dsRNA (IU-dsRNA) specifically accumulates in a SG-like complex and suppresses IFN induction and apoptosis (Scadden, 2007; Vitali and Scadden, 2010). Furthermore, it has been previously demonstrated that IU-dsRNA, in addition to interacting with a protein complex largely comprising components of cytoplasmic SGs, also interacts with proteins that are not known to have a role in SG formation (Callebaut and Mornon, 1997; Scadden, 2005; Yang et al., 2007). Recent work has shown that Z_α domains in isolation associate with SGs and can drive proteins to localize there (Ng et al., 2013). These results suggest that Z_α domains may be responsible for the localization of ADAR1 and DAI in SGs. Nevertheless, the mechanism of SG association, and the interactions of Z_α domains and other constituents within SGs, are unknown.

Here we use the N-terminal part of human DAI ($Z_{\alpha\beta}^{DAI}$), which consists of two tandemly repeated Z_α domains, to study its interactions with nucleic acids and localization, as well as to characterize the complexes in which Z_α domains participate under conditions of arsenite-induced stress. Our results, using *in vitro* and *in vivo* approaches, indicate that the mechanism for the translocation

Journal of Cell Science (2021) 134, jcs258446. doi:10.1242/jcs.258446

of Z_α domain-containing proteins to SGs is mainly mediated by the nucleic acid-binding ability of their Z_α domains.

RESULTS

$Z_{\alpha\beta}^{DAI}$ binds to hyperedited nucleic acids enriched in SGs

DNA-dependent activator of IFN-regulatory factors (DAI) activates type I IFN in response to foreign DNA. The DAI protein contains two tandemly repeated Z_α domains (referred to individually as Z_α and Z_β) and a DNA-binding region (D3) at its N-terminus (Fig. 1A). Note that the D3 region overlaps with the RHIM-like repeat (RLR) A (Kaiser et al., 2008). Furthermore, the Z_β domain name is used to differentiate this domain from Z_α, and unlike the Z_β domain of ADAR1, Z_β of DAI is nucleic acid-binding proficient. Upon activation, the C terminus of DAI binds to a serine/threonine kinase and to IRF3, a transcription factor. The N-terminal region, including D3, is thought to be essential for sensing DNA, as shown by its ability to bind to Z-DNA and synthetic B-DNA (Takaoka et al., 2007). As our primary investigation, we assessed the ability of the wild-type (WT) DAI N-terminal region ($Z_{\alpha\beta}^{DAI}$) and mutant $Z_{\alpha\beta}^{DAI}$ (which was mutated in key residues involved in nucleic acid binding) to bind to $d(CG)_7$ (an oligonucleotide that can adopt the Z conformation) *in vitro*. As evident from electrophoretic mobility shift assay (EMSA) analysis, the WT $Z_{\alpha\beta}^{DAI}$ protein could bind to the $d(CG)_7$ oligonucleotide, whereas the mutant $Z_{\alpha\beta}^{DAI}$ protein showed no binding (Fig. 1D). This clearly demonstrates that mutation of the residues implicated in nucleic acid-binding abolishes the ability of $Z_{\alpha\beta}^{DAI}$ to bind to canonical Z-conformation-adopting nucleic acids.

Another Z_α domain-containing protein, ADAR1, is responsible for the hyperediting of nucleic acids. Apart from widespread A-to-I RNA editing of Alu-containing mRNAs in the human transcriptome (Athanasiadis et al., 2004), it has been speculated that ADAR1 has roles in editing foreign nucleic acids and RNAs sequestered within SGs (Weissbach and Scadden, 2012). To test the ability of WT $Z_{\alpha\beta}^{DAI}$ protein to bind to hyperedited nucleic acids, we synthesized Z-conformation-adopting (purine-pyrimidine repeat-containing) oligonucleotides with thymine-inosine (TI) and cytosine-inosine (CI) repeats and assessed their binding with $Z_{\alpha\beta}^{DAI}$ *in vitro* (Table S6). Poly(I:C) dsRNA triggers the IFN-γ pathway, whereas poly(I:U) dsRNA suppresses the induction of interferon-stimulated genes (ISGs) and apoptosis in response to poly(I:C) (Perrot et al., 2010; Vitali and Scadden, 2010). $Z_{\alpha\beta}^{DAI}$ was found to bind to all these oligonucleotides with variable affinity (Fig. 1E). Any break in the purine-pyrimidine repeat motif for shorter oligonucleotides led to poorer binding, as was evident for the TI1 and CI2 oligonucleotides (Fig. 1E). These results provide the first *in vitro* proof that WT $Z_{\alpha\beta}^{DAI}$ binds to hyperedited Z-conformation-adopting nucleic acids that are likely enriched in SGs, whereas the mutant $Z_{\alpha\beta}^{DAI}$ shows no binding whatsoever.

The $Z_{\alpha\beta}^{DAI}$ domain localizes to SGs

ADAR1 and DAI, the two mammalian proteins that contain Z_α domains, localize to cytoplasmic RNPs known as SGs (Deigendesch et al., 2006; Weissbach and Scadden, 2012). Previous work from us and others has suggested that isolated Z_α domains also localize to SGs (Kuś et al., 2015; Ng et al., 2013) and thus may be responsible for the localization of the proteins that contain them. To further explore the specific subcellular distribution of Z_α domains, their nucleic acid targets and potential protein interactors, we constructed A549 cells stably expressing a GFP fusion to the N-terminal 164 amino acids of the nucleic acids sensor DAI, which contains two Z_α domains. We expressed this GFP–$Z_{\alpha\beta}^{DAI}$ fusion in stably transfected A549 cells and determined the distribution of the protein under different growth conditions. Under unperturbed conditions, the GFP–$Z_{\alpha\beta}^{DAI}$ fusion showed a diffuse distribution in both the cytoplasm and nucleus (Fig. 2A, bottom). When cells were treated with arsenite, WT $Z_{\alpha\beta}^{DAI}$ became enriched in cytoplasmic granules (Fig. 2A, top) that we identified as SGs based on staining for TIAR (also known as TIAL1; Fig. 2A, top), whereas the mutant $Z_{\alpha\beta}^{DAI}$ remained dispersed in the cytosol, regardless of arsenite treatment (Fig. 2B). We observed GFP colocalization with SGs in 92% of cells expressing GFP–$Z_{\alpha\beta}^{DAI}$ (n=50). Conversely, in cells expressing mutant GFP–$Z_{\alpha\beta}^{DAI}$, less than 2% of the cells showed GFP localizing in SGs (Fig. 2B). In addition, we observed intense GFP staining of a variable number of nuclear foci that resembled paraspeckles in size, shape and distribution (Fig. S1). However, these nuclear structures appeared only after arsenite treatment, suggesting they are components of stress responses. As both SGs and paraspeckles are RNPs, these results suggest that Z_α domains may be binding to RNAs that localize in such bodies.

Interaction partners of $Z_{\alpha\beta}^{DAI}$ and mutant $Z_{\alpha\beta}^{DAI}$ under conditions of stress

To understand whether $Z_{\alpha\beta}^{DAI}$ localizes to SGs specifically to perform a role in SG physiology or, alternatively, associates with SGs due to a secondary effect resulting from its affinity for ribonucleic acid, we decided to characterize the components of Z_α complexes. Immunoprecipitation (IP) was performed employing anti-GFP beads, and the resulting IPs were then used to identify proteins involved in $Z_{\alpha\beta}^{DAI}$ complexes. Triplicate IPs were performed from cells expressing either GFP–$Z_{\alpha\beta}^{DAI}$, a GFP fusion to a $Z_{\alpha\beta}^{DAI}$ quadruple mutant with abolished nucleic acid binding or GFP alone. Each IP was performed with arsenite treatment, and all samples were then subjected to liquid chromatography-tandem mass spectrometry (LC-MS/MS) analysis. $Z_{\alpha\beta}^{DAI}$ and $Z_{\alpha\beta}^{DAI}$ quadruple mutant interactomes were normalized with respect to the GFP-alone control. Fig. 3A shows a volcano plot depicting the statistical significance and differential enrichment of proteins in the interactome for WT $Z_{\alpha\beta}^{DAI}$ compared to that for GFP alone, and Fig. 3B shows the same analysis for the $Z_{\alpha\beta}^{DAI}$ quadruple mutant (summarized in Tables S2 and S3, respectively). The top significant interactors were all found to be RNA-binding proteins. The three strongest hits were tRNA-splicing ligase RtcB homolog (RTCB), 40S ribosomal protein S19 and nucleolin. These proteins interact independently of whether the nucleic acid-binding ability of the $Z_{\alpha\beta}^{DAI}$ protein was mutated, suggesting a direct protein interaction. Other proteins that were found as potential interacting partners of both WT and mutant $Z_{\alpha\beta}^{DAI}$ were those that are involved in translation (ribosomal subunits), ATP-dependent RNA helicase activity (DDX5, DDX1 and DDX17) and mRNA transport (Ras GTPase-activating protein-binding protein 2, also known as G3BP2), as well as RNA-binding proteins like p54nrb (also known as NONO), SFPQ (also known as PTB-associated splicing factor, PSF), RNA-binding protein 14, nuclear fragile X mental retardation-interacting protein 2, HEXIM1, heterogeneous nuclear ribonucleoprotein U-like protein 1 (HNRNPUL1), ataxin-2-like protein, alpha-adducin and FUS. Interestingly, although p54nrb and FUS are known components of nuclear paraspeckles (Fox and Lamond, 2010), they have also been shown to localize to neuronal cytoplasmic RNP granules (Furukawa et al., 2015). Furthermore, we found that interactions with proteins of the small 40S ribosomal subunit (S2, S4, S18 and S19 for WT $Z_{\alpha\beta}^{DAI}$; S2, S5, S6, S11, S14, S18 and S19 for mutant $Z_{\alpha\beta}^{DAI}$) were slightly overrepresented as compared to those with proteins of the large 60S ribosomal subunit (P0 and P1 for WT $Z_{\alpha\beta}^{DAI}$; L26, P0, L19, L8 and P1 for mutant $Z_{\alpha\beta}^{DAI}$). It has been previously demonstrated that small, but not large, ribosomal subunits are preferentially recruited to SGs, as

Journal of Cell Science (2021) 134, jcs258446. doi:10.1242/jcs.258446

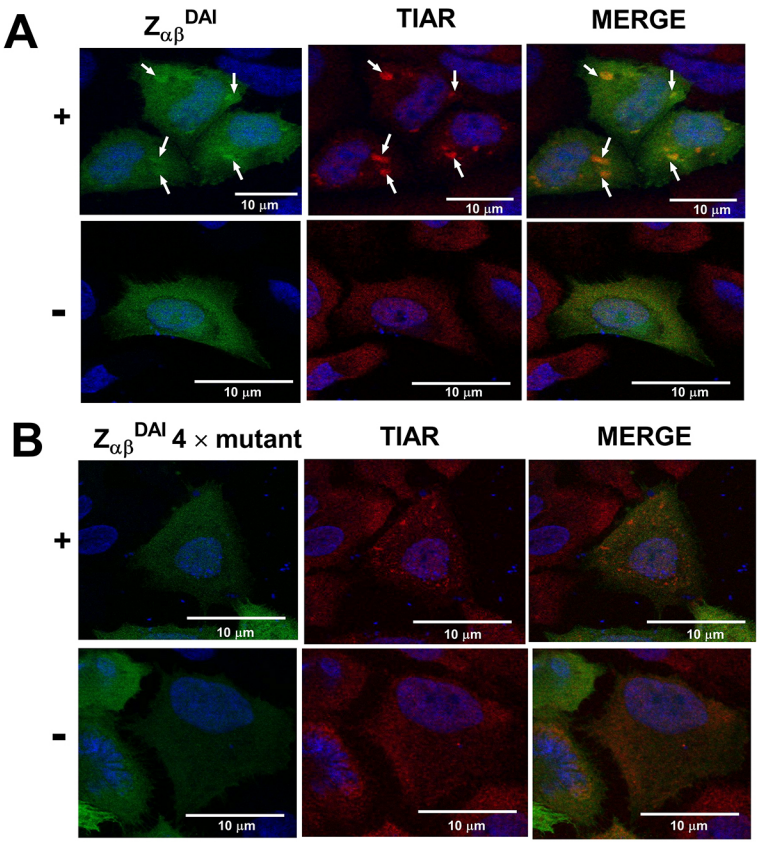

Fig. 2. $Z_{\alpha\beta}^{DAI}$ is enriched in SGs. (A) Immunolocalization of GFP–$Z_{\alpha\beta}^{DAI}$ fusion (green) in the presence (+) and absence (–) of stress induced by arsenite in A549 cells. GFP–$Z_{\alpha\beta}^{DAI}$ localizes to SGs under conditions of stress (top panels, indicated by arrows). Absence of stress leads to diffuse localization of the protein in both cytoplasm and nucleus (bottom panels). The nucleus is stained with DAPI (blue). TIAR (red) is used as a marker protein for SGs. (B) Immunolocalization of mutant GFP–$Z_{\alpha\beta}^{DAI}$ (N46A/Y50A/N141A/Y145A; $Z_{\alpha\beta}^{DAI}$ 4× mutant) fusion in the presence (+) and absence (–) of stress induced by arsenite in A549 cells. Mutant GFP–$Z_{\alpha\beta}^{DAI}$ loses the ability to significantly colocalize with TIAR in the SGs under conditions of arsenite-induced stress. The experiment was carried out with *n*=3 biological replicates. The individual panels and the merged images generated using ImageJ version 1.50i.

shown by immunofluorescence studies using TIAR as the SG marker (Kedersha et al., 2002). Enrichment of ribosomal proteins also suggests that the RNAs bound by $Z_{\alpha\beta}^{DAI}$ were translationally engaged and, thus, were potentially associated with ribosomes. Another plausible explanation for the presence of ribosomal proteins could be the demonstrated affinity of the Z_{α} domain of ADAR1 for ribosomal RNA segments (Feng et al., 2011). Although all of the reported interactions were normalized with respect to those shown by GFP alone, it is possible that some of the low-confidence interactions may not have physiological relevance. Taken together, our results show that both $Z_{\alpha\beta}^{DAI}$ and the $Z_{\alpha\beta}^{DAI}$ quadruple mutant preferentially bind to RNA-binding proteins.

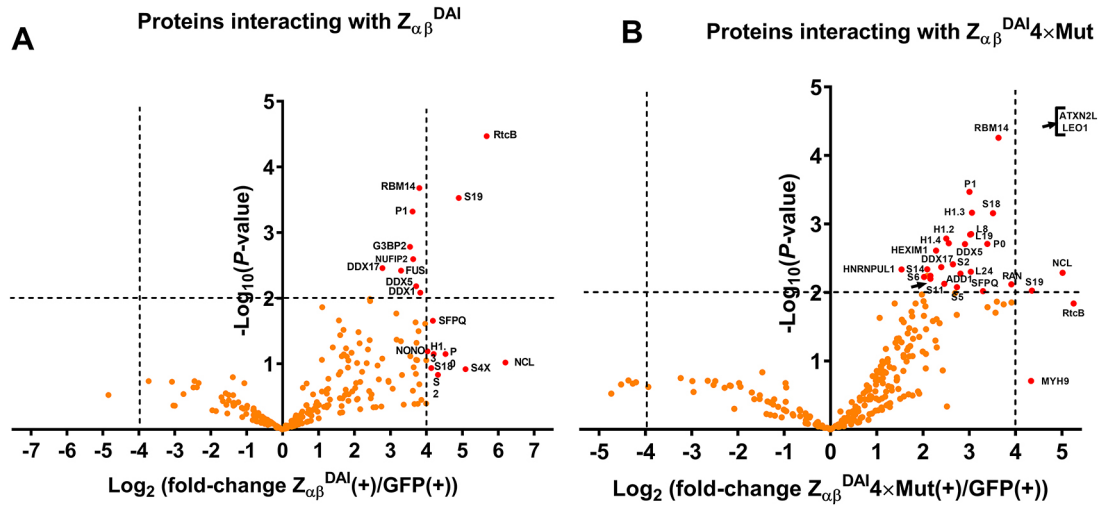

Fig. 3. Interaction partners of $Z_{\alpha\beta}^{DAI}$ protein, normalized with respect to GFP-only control, under conditions of stress induced by arsenite. (A) GFP–$Z_{\alpha\beta}^{DAI}$ versus GFP, under conditions of arsenite-induced stress (+). (B) GFP–$Z_{\alpha\beta}^{DAI}$ quadruple mutant ($Z_{\alpha\beta}^{DAI}$ 4×Mut) versus GFP, under conditions of arsenite-induced stress. The proteomics data in A and B is plotted as volcano plots showing the negative log of *P*-values computed from a pairwise *t*-test for each individual interacting protein on the *y* axis and the $\log_2$ fold change in binding for a particular partner with respect to the GFP-only control on the *x* axis. Data around the origin of the plot represent ∼1-fold change and a *P*-value approaching 1, indicating no significant change, whereas points in the upper-right and upper-left quadrants indicate significantly increased and decreased binding with respect to the controls, respectively. The thresholds (dashed lines) indicate a *P*-value cut-off of 0.01 (*y* axis) and a highly stringent fold change of 16 (*x* axis). Dots coloured red are those that are significant with respect to the abovementioned thresholds. Arrow indicates the position of proteins ATXN2L and LEO1. Fold change values are the mean of three replicate experiments. The statistical analysis and the plots were generated using GraphPad Prism version 7.02.

Journal of Cell Science (2021) 134, jcs258446. doi:10.1242/jcs.258446

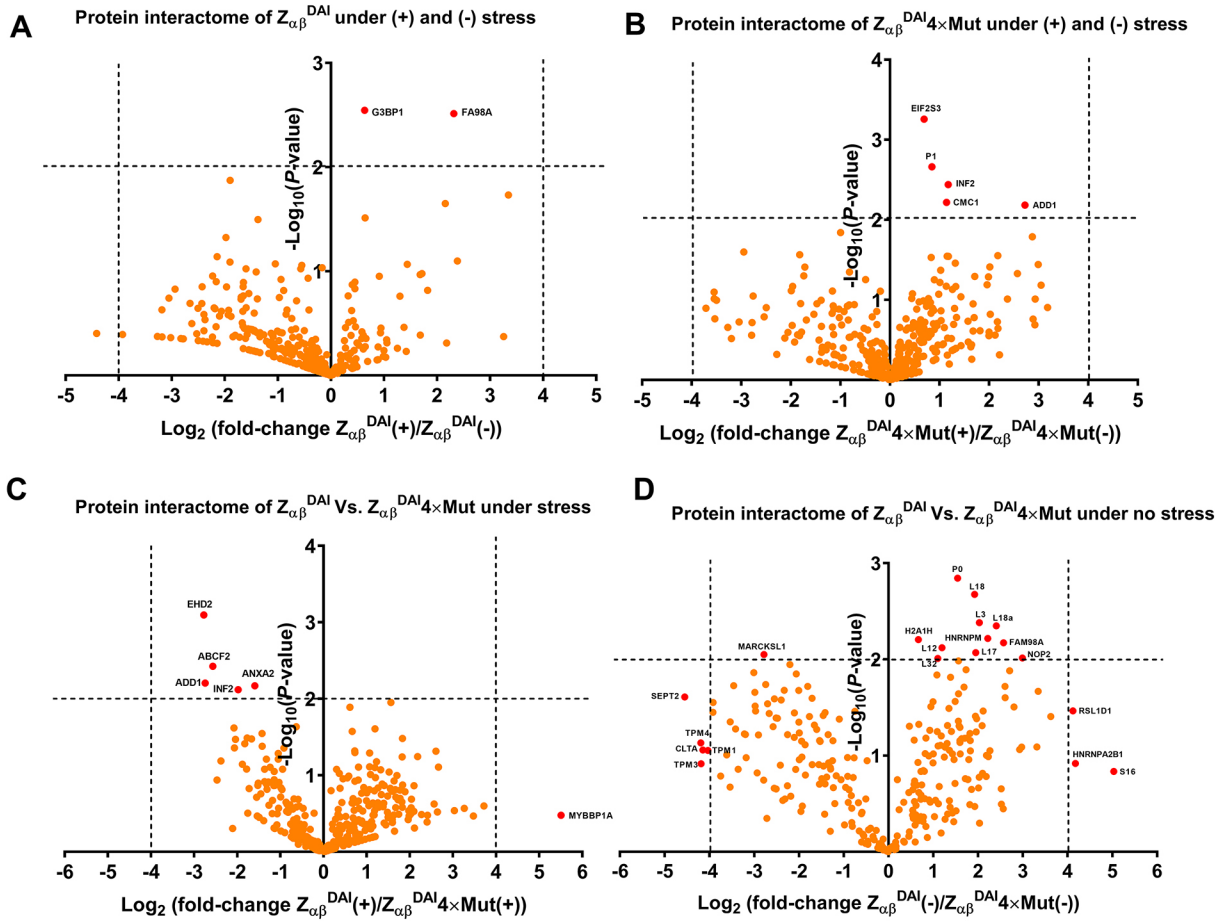

Fig. 4. Differential interactions of $Z_{\alpha\beta}^{DAI}$ and mutant $Z_{\alpha\beta}^{DAI}$ with cellular proteins in the presence and absence of arsenite-induced stress. (A) Comparison of WT GFP–$Z_{\alpha\beta}^{DAI}$ interactomes in the presence (+) or absence (−) of arsenite-induced stress. (B) Comparison of mutant GFP–$Z_{\alpha\beta}^{DAI}$ ($Z_{\alpha\beta}^{DAI}$ 4×Mut) interactomes in the presence or absence of arsenite-induced stress. Volcano plots in panels A and B provide specific insights into SG-mediated interactions. (C,D) Differential interactions with cellular proteins shown by the GFP-tagged WT and mutant $Z_{\alpha\beta}^{DAI}$ in the (C) presence or (D) absence of stress induced by arsenite. Volcano plots provide insights into the interaction enrichment facilitated by the nucleic acid-binding ability of the proteins. The volcano plots were plotted as specified in the Materials and Methods section, and the thresholds identifying the significance of interactions are as discussed in the legend to Fig. 2. Fold change values are the mean of three replicate experiments. The statistical analysis and the plots were generated using GraphPad Prism version 7.02.

The predominant interactions between $Z_{\alpha\beta}^{DAI}$ and SG components are independent of stress

To understand whether the induction of stress or its absence significantly changes the nature of the $Z_{\alpha\beta}^{DAI}$ interactome, IPs were performed with $Z_{\alpha\beta}^{DAI}$ and $Z_{\alpha\beta}^{DAI}$ quadruple mutant in the presence and absence of stress induced by arsenite, and the resulting protein interactors were analysed by LC-MS. Fig. 4A and B show the volcano plots for $Z_{\alpha\beta}^{DAI}$ and the $Z_{\alpha\beta}^{DAI}$ quadruple mutant, respectively, in the presence and absence of arsenite-induced stress, and Table S4 summarizes the results for the test–control pairs. This analysis revealed that there is no major difference when comparing the interactome in the absence and presence of stress induced by arsenite. This indicates that arsenite-induced stress is not a major driver for selective protein binding to the $Z_{\alpha\beta}^{DAI}$ domain. Although there are a few proteins that show statistically significant association with respect to their control pair, none of the hits showed both statistical significance and substantial ratiometric fold enrichment. However, it is noteworthy that the WT $Z_{\alpha\beta}^{DAI}$ showed preferential association with Ras GTPase-activating protein-binding protein 1 (G3BP1), an SG effector that can induce SG assembly upon overexpression (Tourrière et al., 2003), and FAM98A, an RNA-binding protein that has been found in complex with an ATP-dependent RNA helicase, DDX1, and C14orf166 (Akter et al., 2017; Pérez-González et al., 2014).

The mutant $Z_{\alpha\beta}^{DAI}$, on the other hand, showed preferential interaction with eukaryotic translation initiation factor 2 subunit 3, 60S acidic ribosomal protein P1, inverted formin-2, COX assembly mitochondrial protein homolog and alpha-adducin under conditions of stress induced by arsenite.

These findings likely reflect the fact that the $Z_{\alpha\beta}^{DAI}$ that accumulates in SGs represents only a small fraction of the total pool, and hence the predominant interactions between $Z_{\alpha\beta}^{DAI}$ and other proteins are stress independent. Thus, it might be reasonable to assume that $Z_{\alpha\beta}^{DAI}$ may be pre-bound to diffuse mRNA/ribosome-associated complexes that translocate to SGs upon stress induction. Methodologies to specifically isolate SGs are needed to clarify whether there are additional partners of $Z_{\alpha\beta}^{DAI}$ that are specific to the stress granule environment. Furthermore, the partners reported here are likely specific interactors given that TIAR, a key component of SGs, is completely absent in the proteomics data obtained from IPs. This also suggests that the complexes formed by $Z_{\alpha\beta}^{DAI}$ are diffusely distributed and are likely distinct from the corresponding RNPs.

Journal of Cell Science (2021) 134, jcs258446. doi:10.1242/jcs.258446

Interaction of $Z_{\alpha\beta}^{DAI}$ with other proteins is principally mediated by their nucleic acid-binding ability

Comparison of the interactomes of WT $Z_{\alpha\beta}^{DAI}$ and mutant $Z_{\alpha\beta}^{DAI}$, which lacks the ability to bind nucleic acids, showed that the bulk of the interactions with ribosomal proteins are mediated by nucleic acid-binding ability of the $Z_{\alpha\beta}^{DAI}$ domain (Fig. 4C,D; Table S5). Although the results under conditions of arsenite-induced stress were less clear, analysis of the interaction profiles of WT and mutant $Z_{\alpha\beta}^{DAI}$ under physiological conditions (no stress) revealed a set of proteins interacting with $Z_{\alpha\beta}^{DAI}$ in a manner dependent on its nucleic acid-binding capacity (Fig. 4D). Under conditions of no arsenite stress, the WT protein showed a statistically significant difference in interaction with 14 proteins, all of which were nucleic acid-binding proteins. These proteins include those that constitute the 60S and 40S ribosomal subunits, histones and heterogenous nuclear ribonucleoproteins. In complete contrast, the mutant protein showed statistically significant difference in interaction with six proteins, none of which have been implicated in functions related to RNA binding (Table S5). It should be emphasized that even when a lower cut-off of 2-fold enhancement of interaction ($\log_2$ fold-enhancement=1) was applied at the same *P*-value threshold, the same patterns were followed, whereby all the interactions shown by the WT $Z_{\alpha\beta}^{DAI}$ domain were proteins with nucleic acid-binding ability, whereas most interacting partners specific to the mutant were not nucleic acid-binding proteins (Table S5). This finding unambiguously points to the importance of the nucleic acid-binding ability of $Z_{\alpha\beta}^{DAI}$ as the principal driving force behind its interaction with other nucleic acid-binding proteins.

Confirmation of the interaction between $Z_{\alpha\beta}^{DAI}$ and the SG components FUS and p54nrb using immunoprecipitation and immunofluorescence

To confirm the interaction of $Z_{\alpha\beta}^{DAI}$ protein with components of SGs, as revealed by our mass spectrometry analysis, we selected two prominent SG-associated proteins, FUS and p54nrb. Attempts to probe for SFPQ were not undertaken, because this protein is highly similar to p54nrb (antibodies against the two proteins cross react) and forms heterodimers with the latter (Yarosh et al., 2015). Western blotting of IP samples was performed under the same conditions as used for the mass spectrometry characterization experiments, using GFP-tagged $Z_{\alpha\beta}^{DAI}$. Both FUS and p54nrb were detected in the corresponding IPs (Fig. 5). Both proteins were mostly found in the unbound fraction of the IP, suggesting that only a fraction of these proteins associates with $Z_{\alpha\beta}^{DAI}$. This is expected, as both proteins have localizations distinct from that of $Z_{\alpha\beta}^{DAI}$ and have been reported to be primarily localized in the nucleus (Shelkovnikova et al., 2014). To understand whether the interaction was dependent on the presence of a nucleic acid intermediate, we performed similar IPs from extracts treated with an RNAse cocktail (Fig. 5). Interestingly, p54nrb was lost in RNAse-treated samples, suggesting an RNA-mediated interaction (Fig. 5A). However, the levels of FUS were significantly increased upon RNAse treatment, pointing to a protein–protein interaction with $Z_{\alpha\beta}^{DAI}$, at least under these conditions. As a control, we performed IPs from cells expressing either GFP-tagged mutant $Z_{\alpha\beta}^{DAI}$ or GFP alone. FUS was only weakly detected in IP samples from cells expressing the mutant $Z_{\alpha\beta}^{DAI}$ protein, and p54nrb was not detected in these samples (Fig. 5A,B). The GFP IPs showed no p54nrb or FUS, suggesting that their interaction with $Z_{\alpha\beta}^{DAI}$ is specific (Fig. 5). The ability of the mutant $Z_{\alpha\beta}^{DAI}$ to interact with FUS, though weak, was unexpected and suggests that the nucleic acid-binding activity, to some extent, may be required for the FUS interaction, despite this not being mediated by RNA. This indicates that a direct protein–protein interaction is, perhaps allosterically, affected by the engineered mutations or that the RNA and protein interaction surfaces overlap.

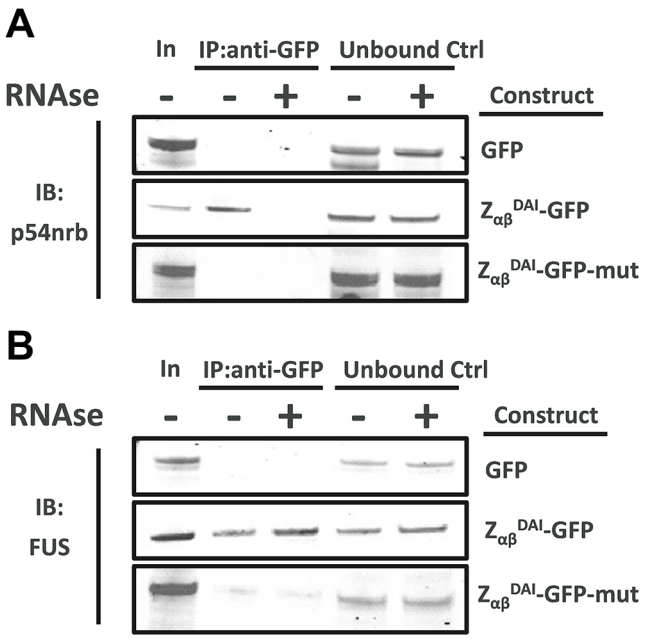

Fig. 5. p54nrb forms an RNA-dependent complex with $Z_{\alpha\beta}^{DAI}$. (A) IP of GFP–$Z_{\alpha\beta}^{DAI}$ ($Z_{\alpha\beta}^{DAI}$–GFP; middle panel) and mutant GFP $Z_{\alpha\beta}^{DAI}$ ($Z_{\alpha\beta}^{DAI}$–GFP-mut; bottom panel) from the lysate of A549 cells, using GFP-trap, that were immunoblotted (IB) with antibodies against p54nrb. The GFP control is shown in the top panel. As seen, p54nrb forms an RNA-dependent complex with $Z_{\alpha\beta}^{DAI}$, because treatment with RNAse results in complete absence of p54nrb from the blot. (B) IP of GFP–$Z_{\alpha\beta}^{DAI}$ (middle panel) and mutant GFP–$Z_{\alpha\beta}^{DAI}$ (bottom panel) from the lysate of A549 cells that were immunoblotted using antibodies against FUS. The GFP control is shown in the top panel. As seen, FUS forms an RNA-independent complex with $Z_{\alpha\beta}^{DAI}$, because treatment with RNAse does not change the level of FUS in the blot. However, the results with the mutant are unexpected given that the mutant $Z_{\alpha\beta}^{DAI}$ (lacking *in vitro* nucleic acid-binding ability) should pull down FUS to the same extent as WT $Z_{\alpha\beta}^{DAI}$. In, input. The experiments were performed in triplicate with almost identical outcomes.

Next, we aimed to determine where in the cells the $Z_{\alpha\beta}^{DAI}$–FUS–p54nrb–SFPQ complex resides. These proteins are known to be localized in the nucleus and have been previously been found enriched in paraspeckles (Shelkovnikova et al., 2014), thus we wondered whether the nuclear speckles observed to accumulate in $Z_{\alpha\beta}^{DAI}$–GFP-expressing cells are paraspeckles. To test this, we co-stained A549 cells expressing GFP–$Z_{\alpha\beta}^{DAI}$ with anti-GFP and antibodies against FUS or p54nrb. Neither FUS nor p54nrb were found to be enriched in $Z_{\alpha\beta}^{DAI}$ nuclear foci (Fig. S2). Both FUS and p54nrb showed a diffuse nuclear staining, and although we cannot exclude their presence in $Z_{\alpha\beta}^{DAI}$ speckles, there was no indication of a preferred localization in these structures. These results suggest that $Z_{\alpha\beta}^{DAI}$ speckles do not represent paraspeckles. This notion is further supported by staining for PSPC1, another common marker for paraspeckles, which also did not show any specific enrichment in $Z_{\alpha\beta}^{DAI}$ nuclear speckles (Fig. S2).

While we could not detect any specific colocalization of $Z_{\alpha\beta}^{DAI}$ with FUS and p54nrb in the nucleus, both proteins were enriched in $Z_{\alpha\beta}^{DAI}$ foci in the cytoplasm of arsenite-treated cells (Fig. 6). However, in the absence of stress induced by arsenite, FUS and p54nrb were found to be mostly nuclear with very faint cytosolic presence (Fig. S4). Thus, under conditions of stress, FUS and p54nrb are enriched in SGs, similar to what was observed for

Journal of Cell Science (2021) 134, jcs258446. doi:10.1242/jcs.258446

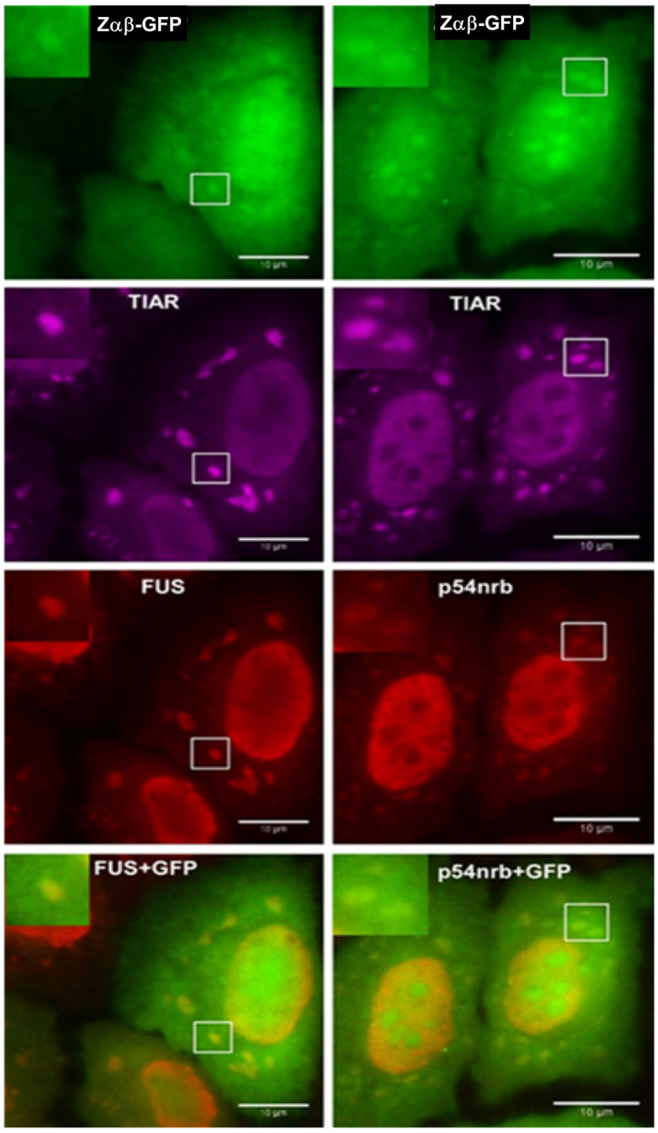

Fig. 6. Both p54nrb and FUS are enriched in SGs along with $Z_{\alpha\beta}^{DAI}$. Arsenite-treated GFP–$Z_{\alpha\beta}^{DAI}$-expressing A549 cells show enrichment of GFP–$Z_{\alpha\beta}^{DAI}$ (Zαβ-GFP; green) in cytoplasmic aggregates that are identified as SGs by co-staining for TIAR (magenta). The same cytoplasmic bodies are stained by anti-p54nrb and anti-FUS antibodies, despite an intense nuclear localization for both these proteins. Boxes indicate regions shown in enlarged inset images. Images shown are representative of three experiments. Scale bars: 10 µm.

$Z_{\alpha\beta}^{DAI}$. The presence of FUS in SGs has been described previously (Aulas and Velde, 2015), and such presence is known to be enhanced in disease conditions associated with neurodegenerative disorders (Shelkovnikova et al., 2014). On the other hand, p54nrb and SFPQ are not commonly found to be present in SGs, except, thus far, in mouse retinal cell lines (Furukawa et al., 2015). Thus, our results point to a possible novel p54nrb–SFPQ function at SGs.

$Z_{\alpha\beta}^{DAI}$ foci represent a novel nuclear structure

Apart from cytoplasmic SGs, $Z_{\alpha\beta}^{DAI}$ also localizes to nuclear speckles (Fig. S1). However, the physiological significance of such localization is not clear, because none of the proteins known to contain Z_α domains are localized in the nucleus. It is likely that the $Z_{\alpha\beta}^{DAI}$ protein localizes to the nucleolus because it contains high concentrations of ribosomal RNAs, which $Z_{\alpha\beta}^{DAI}$ can bind to with high affinity (Feng et al., 2011). However, we decided to explore this localization further, because it suggested that $Z_{\alpha\beta}^{DAI}$ could be utilized as a novel nuclear marker for possibly unique nuclear substructures. Comparison of the nuclear localization of $Z_{\alpha\beta}^{DAI}$ with that of the paraspeckle markers p54nrb and FUS showed that $Z_{\alpha\beta}^{DAI}$ does not colocalize with either of these proteins in the nucleus (Fig. S2), suggesting that the nuclear structures enriched in $Z_{\alpha\beta}^{DAI}$ do not represent paraspeckles. We decided to examine whether the nuclear structures enriched in $Z_{\alpha\beta}^{DAI}$ coincide with another known nuclear structure, such as PML bodies and Cajal bodies, whose general properties are consistent with the ones observed for $Z_{\alpha\beta}^{DAI}$ speckles. However, co-staining of arsenite-treated cells with either anti-PML or anti-coilin antibodies suggested that, despite their close resemblance, $Z_{\alpha\beta}^{DAI}$ bodies are indeed distinct structures (Fig. S3). To our knowledge, $Z_{\alpha\beta}^{DAI}$ bodies are the first nuclear structure whose formation is induced by stress. Although other structures such as PML bodies are responsive to stress, their formation is not stress dependent. Given that the presumed function of Z_α domains appears to be in the cytoplasm, it is not clear that the accumulation of $Z_{\alpha\beta}^{DAI}$ in these structures is physiologically relevant, and we cannot exclude that they are mediated by the GFP tag. Nevertheless, Z_α domains may prove a valuable tool to characterize a novel nuclear structure of relevance to immune and stress responses.

DISCUSSION

The ADAR1 Z_α domain was discovered in an *in vitro* screen that aimed to identify Z-DNA-binding proteins (Herbert and Rich, 1993; Herbert et al., 1997). Whether the ability of the domain to bind to Z-DNA is linked to its *in vivo* function or is coincidental has been a lingering question that is not yet fully resolved. Support for the *in vivo* significance of Z_α domain binding to the left-handed helical conformation of nucleic acids has come from the discovery of other proteins with Z_α domains and the demonstration that all these domains behave similarly *in vitro* and share invariant amino acids that are crucial for Z-DNA binding (Fig. 1A; Schwartz et al., 2001). Crucially, replacement of E3L Z_α domains with those of ADAR1 or DAI has shown that these domains can functionally replace each other, and mutagenesis in this context has shown that amino acids crucial for Z-DNA binding are also essential for the *in vivo* function (Kim et al., 2003).

Although the interaction of Z_α with Z-DNA has been extensively studied, it has become clear that Z_α domains can interact with the left-handed RNA double helix as well (Placido et al., 2007). Considering the known functions of the proteins that have Z_α domains, an RNA-targeting function appears more likely. The results presented here further support an interaction of Z_α domains with RNA. The enrichment of Z_α domains in SGs, a location of storage for stalled ribosomes and mRNAs, suggests that Z_α domains are pre-bound to mRNAs or ribosomal RNAs that translocate to SGs, resulting in the observed enrichment. It has been suggested that Z_α domains are specifically targeted to SGs (Ng et al., 2013). However, our results do not support this notion, as only a fraction of Z_α was found to localize to SGs, suggesting a passive increase due to RNA enrichment. Indeed, with a few notable exceptions, we did not observe major differences in the proteins that interact with the Z_α domain and RNA in the presence or absence of stress. A pertinent question is, however, whether our approach is suitable for detecting the total proteome that the $Z_{\alpha\beta}^{DAI}$ protein interacts with, as SGs are dynamically assembled by the transient and weak interactions that characterize liquid–liquid phase-separated compartments (Guillén-Boixet et al., 2020). Under conditions of stress, the interactome we

Journal of Cell Science (2021) 134, jcs258446. doi:10.1242/jcs.258446

identified under highly stringent volcano plot thresholds predominantly consisted of markers of SGs, and this approach gives us the confidence that slight relaxation of the thresholds is adequate to detect a rich repertoire of specific interactions under the conditions of stress and no stress. However, future experiments using proximity-dependent biotinylation approaches coupled with mass spectrometry could help uncover the overlapping and discrepant fractions of the accessible interactome by these different methodologies.

All the top interacting proteins we identified are previously known RNA-interacting proteins with key roles in RNA processing and trafficking. Among them, p54nrb is of particular interest as it has been previously indirectly linked to ADAR proteins and Z_α by results showing its involvement in nuclear retention of heavily edited mRNAs (Prasanth et al., 2005). It has been speculated that p54nrb may directly recognize the presence of inosine in such mRNAs, but no direct evidence of this recognition has emerged yet. This previously described p54nrb interaction with edited transcripts occurs in the nucleus and is linked to the formation of paraspeckles. We found that p54nrb is also present in the cytoplasm, albeit at much lower levels. However, significant amounts of the protein were found in SGs. Whether this fraction of p54nrb originates from a diffuse cytoplasmic distribution or directly migrates from the nucleus is not clear and needs further study. Our experiments suggest that the nuclear $Z_{\alpha\beta}^{DAI}$ speckles are not enriched in p54nrb and are not paraspeckles, and thus this is not likely to be where the p54nrb–$Z_{\alpha\beta}^{DAI}$ complex originates. The identification of SFPQ as a top interactor with $Z_{\alpha\beta}^{DAI}$ is not surprising given the presence of p54nrb; the two proteins are homologues and are known to form heterodimers (Passon et al., 2012), which is consistent with our finding of a similar number of peptides for the two proteins.

FUS shows a localization distribution similar to that of p54nrb, but its translocation to SGs has been previously observed and linked to pathologies leading to neurodegenerative disorders (Li et al., 2013; Masuda et al., 2016). Thus, an interpretation of our results would be that Z_α domains target a subset of mRNAs also targeted by a FUS–p54nrb–SFPQ complex. The function of such a complex and the nature of RNAs targeted are open questions and will be discussed further. Interestingly FUS mutations cause amyotrophic lateral sclerosis (ALS), which leads to cell death of motor neurons (An et al., 2019). Cell death in this disease has been attributed to hypoediting of the GLUR2 (GRIA2) subunit of AMPA receptors leading to a lethal increase of intracellular Ca^{2+} (Da Cruz and Cleveland, 2011). How FUS mutations are linked to changes in editing levels remains unclear. Although GLUR2 editing is mediated by ADAR2 (also known as ADARB1; Peng et al., 2006), changes in ADAR1, which is known to compete with ADAR2 for substrate binding, may influence ADAR2 activity. Thus, our findings provide the first link between FUS and the editing machinery, which might be worth exploring further in the context of ALS. Several other RNA-binding proteins (DDX1, HNRNPUL1, RTCB and C14orf166) were also found to be enriched in $Z_{\alpha\beta}^{DAI}$ IPs, including several helicases and splicing-related proteins, supporting the idea that the entire complex accompanies trafficking mRNAs.

A significant effort has been devoted to characterizing the RNA-binding properties of FUS using CLIP-seq and *in vitro* SELEX analysis, revealing a complex RNA recognition pattern (Wang et al., 2015; Choi et al., 2017). CLIP-seq experiments have shown a recognition of GU-rich motifs. Similarly, SELEX has revealed GGUG-motif recognition, with RNA recognition shown to be direct and mediated by the zinc-finger domain of FUS (Loughlin et al., 2019). Other studies, however, suggest limited specificity and indicate that GU motifs cannot explain the range of RNA-binding interactions of FUS (Wang et al., 2015). RNA binding close to alternative splicing signals and regulation of alternative splicing is the most prevalent functional role assigned to FUS, although links to transcription and polyadenylation have been reported (Masuda et al., 2015). Given the multifunctional role of FUS and the lack of clear specificity, it is possible that specific functions of FUS are mediated by other proteins providing sequence or structural specificity. Our data suggest that the interaction of $Z_{\alpha\beta}^{DAI}$ with FUS includes a protein–protein component, and thus it is tempting to suggest that interactions with Z_α domains may guide the cytoplasmic functions of FUS.

SFPQ and p54nrb, along with PSPC1, form the DHBS family of proteins, which share homology, domains and a multifunctional role centred on splicing and mRNA metabolism (Yarosh et al., 2015). In the nucleus, SFPQ and p54nrb are found in paraspeckles, where they interact with the scaffolding lncRNA Neat1, which forms the basis of paraspeckles. The two proteins have been shown to mediate nuclear retention of heavily edited RNAs by ADAR proteins, and thus their presence as strong interactors with Z_α domains are of particular interest. However, we observed no colocalization of $Z_{\alpha\beta}^{DAI}$ with SFPQ–p54nrb in nuclear structures, suggesting that the signal we detect may come from cytoplasmic complexes. Although SFPQ and p54nrb are primarily nuclear, reports have demonstrated a role of SFPQ in IRES-mediated translation (Sharathchandra et al., 2012) and translocation of SFPQ to the cytoplasm in Alzheimer's and Pick's disease (Ke et al., 2012). Our results showing localization of p54nrb in arsenite-induced SGs emphasize a cytoplasmic role for SFPQ and p54nrb.

What is the nature of the RNAs to which $Z_{\alpha\beta}^{DAI}$ and FUS–p54nrb–SFPQ bind? Given the described affinity of p54nrb–SFPQ for inosine-containing duplexes, it is tempting to speculate that edited RNAs that are not retained in (or escape from) paraspeckles are targeted in the cytoplasm and escorted to SGs upon elevated stress. Since it is known that the ADAR1 Z_α domain targets RNAs that have already been modified in the nucleus (Zhang and Carmichael, 2001), selective targeting of nucleic acid by the enzyme for more extensive modification in the cytoplasm is highly likely. Although the propensity and extent of inosine-containing RNA duplexes to be in the left-handed conformation is not clear, it is tempting to suggest that selective binding of Z_α to the left-handed helical conformation of inosine-containing nucleotides targets proteins to modified duplexes without the need to specifically recognize the inosine base. Our *in vitro* binding data with TI- and CI-repeat oligonucleotides is the first report exploring the interaction of Z_α domains with hyperedited nucleic acids. We now know that the long cytoplasmic form of ADAR1, which contains the Z_α domain, has a crucial role in restoring homeostasis after the activation of the IFN pathway (Gannon et al., 2018). Targeting of ADAR1 specifically to activating RNAs would efficiently reduce cytoplasmic danger signals while avoiding binding and sequestration of the enzyme on innocuous RNAs.

In conclusion, our study shows that Z_α domains interact with both unedited and hyperedited nucleic acids. Furthermore, their localization in SGs is a secondary effect of their interactions with the nucleic acids and RNP complexes that translocate to SGs under conditions of stress.

MATERIALS AND METHODS

Cloning, expression and purification of $Z_{\alpha\beta}^{DAI}$ for *in vitro* studies

A nucleic acid-binding deficient quadruple mutant of the tandemly repeated Z_α domains of DAI was generated using $Z_{\alpha\beta}^{DAI}$ [amino acids 2–165 from the N terminus of human DAI (NM_030776.2)] that was cloned in pET28a vector (Invitrogen) using NheI and XhoI restriction enzymes (Table S7).

Journal of Cell Science (2021) 134, jcs258446. doi:10.1242/jcs.258446

The mutants were generated using the NZYMutagenesis kit (NZYTech). The residue number and the identity of the quadruple mutant that was generated is as follows: $Z_{\alpha\beta}{}^{DAI}$-N46A/Y50A and $Z_{\alpha\beta}{}^{DAI}$-N141A/Y145A (Fig. 1B). The initial round of site-directed mutagenesis using primer 1 and 2 (Table S7) generated a double mutant in the N-terminal Z_{α} domain of $Z_{\alpha\beta}{}^{DAI}$. This double mutant was used as the template for the subsequent round of site-directed mutagenesis (using primer 3 and 4; Table S7) to generate the quadruple mutant.

Expression and purification of the WT and mutant constructs was carried out employing well-established protocols. Briefly, the construct was expressed in *Escherichia coli* strain BL21 (DE3) selected using kanamycin (50 µg/ml). Cell cultures with 0.6–0.9 OD_{600} were induced with 0.4 mM IPTG. After 3–4 h, cells were harvested by centrifugation (5000 ***g***) at 4°C. Chemical cell lysis was performed in 20 mM Tris-HCl pH 7.6, 50 mM NaCl, 5 mM $MgCl_2$ and 1× Bugbuster (Novagen) in the presence of 1 mM PMSF, a mixture of proteinase inhibitors (Complete Mini, EDTA-free; Roche), and benzonase (Novagen) for 1 h at 4°C with constant stirring. The lysed cell culture was centrifuged at 30,597 ***g*** for 30 min, and the supernatant was filtered through a 0.2 µm syringe filter. The protein extract (filtrate) was loaded on a pre-equilibrated HiTrap IMAC-Sepharose FF column (GE Healthcare). The column was then washed with buffer A (50 mM Tris-HCl pH 7.6, 500 mM NaCl, 1 mM β-mercaptoethanol and 30 mM imidazole), and the protein was eluted using a gradient of 30–500 mM imidazole (buffer B). The histidine tag was cleaved using 10 units of thrombin during an overnight dialysis at 4°C against MonoS buffer A (10 mM HEPES, pH 6.9, and 20 mM NaCl). The cleaved protein was loaded on a Mono S 4.6/100 PE column (GE Healthcare). The column was washed with a gradient of 20–120 mM NaCl. The protein was then eluted using buffer B (10 mM HEPES, pH 6.9, and 1 M NaCl), and the fractions were evaluated by SDS–PAGE. Buffer exchange and concentration was performed using Amicon-Ultra centrifugal filters (Merck Millipore). Finally, the protein was concentrated and stored in storage buffer (10 mM HEPES, pH 7.4, and 20 mM NaCl). The homogeneity and purity of the protein preparation was assessed using SDS–PAGE.

Electrophoretic mobility shift assay for assessing nucleic acid binding

The ability of the purified WT and mutant protein to bind DNA was evaluated by electrophoretic mobility shift assay (EMSA) using a $d(CG)_7$ duplex oligonucleotide and oligos containing TI (mimicking UI-containing hyperedited RNA) and CI repeats (Integrated DNA Technologies) at 10 µM (Table S6). The latter two oligonucleotides are mimics of physiological RNA substrates with hyperedited sites. Mixtures of protein and DNA at several ratios were incubated at 37°C for 20 min and then subjected to electrophoresis on non-denaturing polyacrylamide gels (6% gel retardation gel; Invitrogen) and stained first with SyBR GOLD for nucleic acid oligos followed by Coomassie Blue to stain the protein. Appropriate oligo- and protein-only controls were included to objectively interpret the gel shift patterns.

Cloning and mutagenesis for cell-based studies

The amino-terminal region of human DAI ($hZ_{\alpha\beta}{}^{DAI}$, amino acid residues Ala2–Tyr165) was amplified by PCR using a construct of GST-tagged human DAI (originating from NM_030776.2) as a template and primers incorporating XhoI and BamHI restriction sites (Table S1, primers 1 and 2). The digested PCR product was cloned into a pIC113 vector which allowed the insertion of a LAP tag (Cheeseman and Desai, 2005; Li, 2011) at the N terminus providing fused green fluorescent protein (GFP) and an S-tag with a cleavable TEV site between them (plasmid pIC113$hZ_{\alpha\beta}{}^{DAI}$). The entire construct or the LAP tag only (to be used as control) were subcloned into $pBABE^{puro}$ (Morgenstern and Land, 1990) using primers 3–5 (Table S1), and BamHI and SalI restriction sites, yielding plasmids pBABE$Z_{\alpha\beta}{}^{DAI}$ and pBABE*GFP*, respectively. Site-directed mutagenesis was performed using the NZYMutagenesis kit (NZYTech) to mutate four $hZ_{\alpha\beta}{}^{DAI}$ residues known to be critical for nucleic acid binding to alanine ($Z_{\alpha\beta}$-N46A/Y50A and $Z_{\alpha\beta}$-N141A/Y145A). The mutant constructs, pIC113$hZ_{\alpha\beta}{}^{DAI}$4×Mut and pBABE$Z_{\alpha\beta}{}^{DAI}$4×Mut, were generated following the manufacturer's protocol using primers 6–9 (Table S1), resulting in the quadruple mutant $Z_{\alpha\beta}{}^{DAI}$4×Mut.

Cell culture and arsenite treatment

A549 cells (human lung adenocarcinoma) and HEK293-G cells and their derivatives were cultured in Dulbecco's Modified Eagle Medium (DMEM; Thermo Fisher Scientific) supplemented with 10% heat inactivated fetal bovine serum (Gibco, Thermo Fisher Scientific), penicillin (100 U/ml), streptomycin (100 µg/ml) and L-glutamine (2 mM) (complete medium) in a 5% CO_2 humidified incubator at 37°C.

To induce stress granule formation, A549 cells and their derivatives were cultured in Dulbecco's Modified Eagle Medium (DMEM) supplemented with sodium arsenite (0.5 mM) for 30 min in 5% CO_2. Before and after incubation with arsenite, cells were washed three times with PBS. Cells were then left to recover for 30 min in complete medium lacking arsenite.

Transient transfection and generation of stable cell lines

A549 cells were transfected with pIC113$hZ_{\alpha\beta}{}^{DAI}$ or pIC113$hZ_{\alpha\beta}{}^{DAI}$4×Mut using Lipofectamine LTX, PLUS reagent and OptiMEM (Life Technologies) according to manufacturer's instructions. For the generation of stably expressing cell lines, HEK293-GP cells were co-transfected with pBABE$Z_{\alpha\beta}{}^{DAI}$, pBABE$Z_{\alpha\beta}{}^{DAI}$4×Mut or $pBABE^{GFP}$ and pVSV-G using Lipofectamine LTX, PLUS reagent and OptiMEM (Life Technologies), according to the manufacturer's recommended protocol (Morgenstern and Land, 1990). Retroviral particles were collected after 3 days, filtered through 0.45 µm filters (Acrodisc, Pall) and stored at −80°C. These were used to transduce A549 cells in the presence of 8 µg/ml of hexadimethrine bromide (Polybrene, Sigma). Following 24 h of transduction, cells were trypsinized and seeded for selection in complete medium supplemented with 4 µg/ml puromycin (Calbiochem, Merck Millipore). All cell lines were passaged three times before use and kept in culture supplemented with 2 µg/ml puromycin and/or stored in liquid nitrogen.

Antibodies

The following antibodies were used in this study: anti-ZBP1 clone RonoB19 [1:500 for western blotting (WB); 651602; rat; BioLegend], anti-TIAR (C-18) [1:500 for immunofluorescence (IFA); SC-1749; goat; Santa Cruz Biotechnology], anti-NONO (1:500 for IFA and WB; N8664; rabbit; Sigma-Aldrich); anti-FUS (1:100 for IFA, 1:500 for WB; HPA008784; rabbit; Sigma-Aldrich), anti-PSPC1 (N-terminal) (1:250 for IFA; SAB4200068; rabbit; Sigma-Aldrich), anti-PML (1:100 for IFA; ab53773; rabbit; Abcam) and anti-coilin (1:100 for IFA; rabbit; a kind gift from Dr Paulo Navarro-Costa, Instituto Gulbenkian de Ciência, Oeiras, Portugal), all against the human proteins. Secondary fluorophore-coupled antibodies were all from the Alexa Fluor range (Alexa Fluor 568 and Alexa Fluor 647, A10042 and A21469, respectively; 1:1000 for IFA; Life Technologies).

Immunofluorescence staining and confocal microscopy

Cells were fixed in 4% formaldehyde solution in phosphate-buffered saline (PBS) for 20 min at room temperature (RT). After washing with PBS, samples were permeabilized with 0.2% Triton X-100 (v/v) solution in PBS and 1% fetal bovine serum at RT for 7 min. Cells were blocked, and all subsequent immunofluorescence staining (incubation and washes) was performed in PBS containing 1% fetal bovine serum. Cells were then incubated with the corresponding primary antibodies for 1 h at RT or overnight at 4°C (for coilin and PML staining). After three washes, samples were incubated with the respective secondary antibodies and DAPI (Gerbu BiotechniK) for 30 min at RT. Cells were then mounted using Fluoromount-G (eBioscience) mounting medium.

Confocal images were acquired on a Leica SP5 confocal microscope using a 63×1.3 NA oil-immersion objective and employing 405 nm, 488 nm, 568 nm and 633 nm laser lines. Spectral detection adjustments for the emission of DAPI, eGFP, Alexa 568 and Alexa 633 fluorochromes were made using HyD detectors in standard mode. *Z*-stacks were acquired on a Leica high content screening microscope, based on a Leica DMI6000 equipped with a Hamamatsu Flash 4.0 LT sCMOS camera, using a 100×1.44 NA objective; DAPI, eGFP, TRITC and Cy5 fluorescence filter

sets; and controlled with the Leica LAS X software. Images were processed using ImageJ software (NIH).

Immunoprecipitation and western blotting

A549 cells with or without arsenite treatment from 20 15-cm confluent dishes were lysed in lysis buffer (10 mM Tris-HCl pH 7.4, 150 mM NaCl, 0.5 mM EDTA and 0.5% NP40) complemented with 1× protease inhibitors (Pierce Protease Inhibitor Mini Tablets, EDTA-Free; Thermo Fisher Scientific) and 2 U Turbo DNase (Ambion) on ice for 1 h. The resulting cell lysate was centrifuged at 35,541 ***g*** for 20 min at 4°C. Further, the supernatant from the previous round was centrifuged a second time under the same conditions. The lysate was diluted to a total volume of 9 ml with dilution/wash buffer (lysis buffer with 0.05% Tween 20 instead of NP40) supplemented with protease inhibitors. A 100 µl volume of GFP-trap magnetic beads (ChromoTek) were added to the suspension and incubated for 90 min on a roller device. Beads were magnetically separated using a magnetic stand (Merck Millipore) and washed five times with 1 ml ice-cold dilution/wash buffer. The proteins of interest were eluted by cleavage with 10 units of AcTEV protease (Life Technologies) in a buffer containing 50 mM Tris-HCl pH 8.0, 0.5 mM EDTA and 1 mM dithiothreitol (DTT) in a total volume of 60 µl. The mix was incubated for 90 min on ice. For RNAse-treated samples, the supernatant obtained after centrifugation of cell lysate was split in two and then incubated with beads in the presence of either RNAse cocktail (Ambion; 400 U of RNAse T1 and 10 U RNAseA) or 400 U RNAse inhibitor (SuperRNAseIn, Invitrogen). The rest of procedure was similar to that employed for RNAse treatment, except that the dilution/wash buffer contained 5 mM $MgCl_2$. Final samples were stored at −80°C. For western blotting, samples were prepared after addition of 2.5% β-mercaptoethanol to sample buffer (NuPAGE LDS sample buffer, Life Technologies) and boiling for 5 min at 90°C. The samples were electrophoresed on NuPage 4–12% bis-Tris SDS precast gels from Invitrogen. In all cases, Novex sharp pre-stained molecular weight marker (Life Technologies) was loaded for sizing purposes.

Polyacrylamide gels were then blotted on iBlot Gel Transfer Stacks (Nitrocellulose Mini) following manufacturer's instructions for the iBlot transfer device (Invitrogen). Membranes were blocked in blocking buffer (PBS containing 0.1% Tween 20 and 5% milk powder) for 30 min at RT. After three washes (PBS containing 0.1% Tween 20), membranes were incubated with corresponding antibodies for 60 min at RT. Then membranes were washed three times with PBS containing 0.1% Tween 20 then incubated for 30 min at RT with the corresponding secondary antibodies, either IRDye 680RD-conjugated (926-68073, Li-Cor) or DyLight 800-conjugated (039612-145-120, Rockland), at 1:10,000 dilution. Subsequently, the membranes were washed three times in buffer containing PBS with 0.1% Tween 20, and twice in PBS alone. Western blots were imaged using a LI-COR Biosciences Odyssey near-infrared scanner.

Mass spectrometry and data analysis

Sample preparation

The proteomics analyses were performed in the CRG/UPF Proteomics Unit, Centro de Regulación Genòmica (CRG), Universitat Pompeu Fabra (UPF), Barcelona. The CRG/UPF Proteomics Unit is part of the Spanish Platform of Molecular and Bioinformatics Resources (ProteoRed), Instituto de Salud Carlos III (PT13/0001).

Urea was added to the samples to 6 M final concentration, then samples were reduced with DTT (30 nmoles, 1 h, 37°C) and alkylated in the dark with iodoacetamide (60 nmoles, 30 min, 25°C). The resulting protein extract was first diluted 1:6 with 200 mM NH_4HCO_3 and digested with 1 µg of trypsin (Promega, cat.V5113) overnight at 37°C. Finally, the peptide mix was acidified with formic acid and desalted with a MicroSpin C18 column (The Nest Group, Inc) prior to LC-MS/MS analysis.

10% of each sample was analysed using an LTQ-Orbitrap XL mass spectrometer (Thermo Fisher Scientific, San Jose, CA, USA) coupled to an EasyLC [Thermo Fisher Scientific (Proxeon), Odense, Denmark]. Peptides were loaded onto the 2 cm Nano Trap column with an inner diameter of 100 µm packed with C18 particles of 5 µm particle size (Thermo Fisher Scientific) and were separated by reversed-phase chromatography using a 12 cm column with an inner diameter of 75 µm, packed with 1.9 µm C18 particles (Nikkyo Technos Co., Ltd. Japan). Chromatographic gradients started at 97% buffer A and 3% buffer B for 4 min with a flow rate of 300 nl/min, in 1 min increased to 93% buffer A and 7% buffer B, and then gradually increased to 65% buffer A and 35% buffer B in 60 min. After each analysis, the column was washed for 15 min with 10% buffer A and 90% buffer B. Buffer A, 0.1% formic acid in water; buffer B, 0.1% formic acid in acetonitrile.

The mass spectrometer was operated in positive ionization mode with nanospray voltage set at 2.5 kV and source temperature at 200°C. Ultramark 1621 for the FT mass analyser was used for external calibration prior to the analyses. An internal calibration was also performed using the background polysiloxane ion signal at m/z 445.1200. The instrument was operated in DDA mode and full MS scans with 1 micro scans at resolution of 60,000 were used over a mass range of m/z 350–1500 with detection in the Orbitrap. Auto gain control (AGC) was set to 1×10^6, and dynamic exclusion (60 s) and charge state filtering disqualifying singly charged peptides were both activated. In each cycle of DDA analysis, following each survey scan, the top twelve most intense ions with multiple charged ions above a threshold ion count of 5000 were selected for fragmentation at normalized collision energy of 35%. Fragment ion spectra produced via collision-induced dissociation (CID) were acquired in the ion trap, AGC was set to 5×10^4, and an isolation window of 2.0 m/z and maximum injection time of 50 ms were used. All data were acquired with Xcalibur software v2.2.

Raw data processing

All raw files were analysed together using the software MASCOT (Matrix Science). Frequently observed contaminating proteins as reported in Crapome (Mellacheruvu et al., 2013) such as myosin, tropomyosin, keratin, actin, trypsin etc, though reported diligently, were not given any weightage in further analysis. Carbamidomethylation of cysteine was set as a fixed modification (57.021464 Da) and N-acetylation of protein N termini (42.010565 Da) and oxidation of methionine (15.994915 Da) were set as variable modifications. As no labelling was performed, multiplicity was set to 1. During the main search, parent masses were allowed an initial mass deviation of 7 ppm, and fragment ion mass tolerance was set to 0.5 Da. Peptide score match (PSM) and protein identifications were filtered using a target-decoy approach at a stringent false discovery rate (FDR) of 0.01% and a relaxed FDR of 0.05%.

Post-processing

The final score was computed based on the PSM. The final score obtained for each experiment (e.g. $Z_{\alpha\beta}{}^{DAI}$+arsenite, $Z_{\alpha\beta}{}^{DAI}$ –arsenite, $Z_{\alpha\beta}{}^{DAI}$ 4×mut+arsenite, $Z_{\alpha\beta}{}^{DAI}$ 4×mut – arsenite and GFP+arsenite) were arranged in experimental triplicates and the mean and standard deviation of each row, representing values obtained for each unique interacting protein, were computed. Student's t-test was performed comparing the bait pulldown (in triplicates) to its individual bait-specific control group (in triplicates). This control group varied depending on the nature of comparison, that is, proteins (mutant and WT) versus GFP, mutant versus WT, and proteins (mutant and WT) untreated versus treated. This whole procedure of individual clustering, statistical parameter computation and t-test was repeated for every bait. The resulting differences between the $\log_2$ means of the two groups [$\log_2$(bait/background)] and the negative log P-values were plotted as volcano plots using GraphPad Prism v7. A stringent cutoff of 4 was set for $\log_2$ fold-change representing at least 16-fold change of the test with respect to the control group. A value of 2 for –log(P-value), corresponding to $P<0.01$, was employed to ascribe statistical significance. Quadrants are employed for graphical clarity in figures, and tables explicitly state whether the imputed scores are significant statistically (P-value), numerically (fold-change) or additively (both statistical and numerical). Mass spectrometry scores for the replicate experiments are shown in Tables S8–S13.

Acknowledgements

This manuscript is dedicated to the memory of Alekos Athanasiadis, who sadly passed away in August 2020. Though the manuscript is communicated by B.S. for practical purposes, the work was conceived and supervised by A.A. We thank Élio Sucena, Jonathan C. Howard and Mónica Bettencourt-Dias for providing useful comments.

Competing interests
The authors declare no competing or financial interests.

Author contributions
Conceptualization: A.A.; Methodology: L.G., B.S., J.F.M., L.E.T.J.; Validation: B.S., A.A.; Formal analysis: L.G., B.S., K.K.; Investigation: L.G., B.S., K.K.; Resources: B.S., J.F.M., M.J.A., L.E.T.J., A.A.; Data curation: L.G., B.S., K.K., A.A.; Writing - original draft: B.S., A.A.; Writing - review & editing: B.S., M.J.A., L.E.T.J.; Visualization: L.G., B.S., K.K.; Supervision: A.A.; Project administration: B.S., J.F.M.; Funding acquisition: B.S., A.A.

Funding
This work was supported by a Fundação para a Ciência e a Tecnologia (FCT) grant (PTDC/BBB-BEP/3380/2014 to L.G., B.S. and A.A.). B.S. was also supported by H2020 Marie Skłodowska-Curie Actions Individual Fellowship 789565. K.K. was a recipient of Fundação para a Ciência e a Tecnologia PhD grant SFRH/BD/51626/2011. M.J.A. was supported by the grant PTDC/BIA-CEL/32211/2017 awarded by the Fundação para a Ciência e a Tecnologia. L.E.T.J. was supported by EMBO Installation Grant 1818, a European Research Council consolidator grant (ERC-2013-CoG-615638) and a Fundação para a Ciência e a Tecnologia 'Investigador FCT' position.

Peer review history
The peer review history is available online at
https://journals.biologists.com/jcs/article-lookup/doi/10.1242/jcs.258446

References

Akter, K. A., Mansour, M. A., Hyodo, T. and Senga, T. (2017). FAM98A associates with DDX1-C14orf166-FAM98B in a novel complex involved in colorectal cancer progression. *Int. J. Biochem. Cell Biol.* **84**, 1-13. doi:10.1016/j.biocel.2016.12.013

An, H., Skelt, L., Notaro, A., Highley, J. R., Fox, A. H., La Bella, V., Buchman, V. L., Buchman, V. L., Shelkovnikova, T. A. et al. (2019). ALS-linked FUS mutations confer loss and gain of function in the nucleus by promoting excessive formation of dysfunctional paraspeckles. *Acta Neuropathol. Commun.* **7**, 7. doi:10.1186/s40478-019-0658-x

Athanasiadis, A. (2012). Zalpha-domains: At the intersection between RNA editing and innate immunity. *Semin. Cell Dev. Biol.* **23**, 275-280. doi:10.1016/j.semcdb.2011.11.001

Athanasiadis, A., Rich, A. and Maas, S. (2004). Widespread A-to-I RNA editing of Alu-containing mRNAs in the human transcriptome. *PLoS Biol.* **2**, e391. doi:10.1371/journal.pbio.0020391

Aulas, A. and Velde, C. V. (2015). Alterations in stress granule dynamics driven by TDP-43 and FUS: A link to pathological inclusions in ALS? *Front. Cell. Neurosci.* **9**, 423. doi:10.3389/fncel.2015.00423

Callebaut, I. and Mornon, J. P. (1997). The human EBNA-2 coactivator p100: Multidomain organization and relationship to the staphylococcal nuclease fold and to the tudor protein involved in Drosophila melanogaster development. *Biochem. J.* **321**, 125-132. doi:10.1042/bj3210125

Cheeseman, I. M. and Desai, A. (2005). A combined approach for the localization and tandem affinity purification of protein complexes from metazoans. *Sci. STKE.* **266**, pl1. doi:10.1126/stke.2662005pl1

Choi, S. K., Park, C., Kim, K. E. and Kim, K. K. (2017). An in vitro technique to identify the RNA binding-site sequences for RNA-binding proteins. *BioTechniques* **63**, 28-33. doi:10.2144/000114567

Da Cruz, S. and Cleveland, D. W. (2011). Understanding the role of TDP-43 and FUS/TLS in ALS and beyond. *Curr. Opin. Neurobiol.* **21**, 904-919. doi:10.1016/j.conb.2011.05.029

De Rosa, M., De Sanctis, D., Rosario, A. L., Archer, M., Rich, A., Athanasiadis, A. and Carrondo, M. A. (2010). Crystal structure of a junction between two Z-DNA helices. *Proc. Natl. Acad. Sci. USA* **107**, 9088-9092. doi:10.1073/pnas.1003182107

De Rosa, M., Zacarias, S. and Athanasiadis, A. (2013). Structural basis for Z-DNA binding and stabilization by the zebrafish Z-DNA dependent protein kinase PKZ. *Nucleic Acids Res.* **41**, 9924-9933. doi:10.1093/nar/gkt743

Deigendesch, N., Koch-Nolte, F. and Rothenburg, S. (2006). ZBP1 subcellular localization and association with stress granules is controlled by its Z-DNA binding domains. *Nucleic Acids Res.* **34**, 5007-5020. doi:10.1093/nar/gkl575

Feng, S., Li, H., Zhao, J., Pervushin, K., Lowenhaupt, K., Schwartz, T. U. and Dröge, P. (2011). Alternate rRNA secondary structures as regulators of translation. *Nat. Struct. Mol. Biol.* **18**, 169-177. doi:10.1038/nsmb.1962

Fox, A. H. and Lamond, A. I. (2010). Paraspeckles. *Cold Spring Harb. Perspect. Biol.* **2**, a000687. doi:10.1101/cshperspect.a000687

Furukawa, M. T., Sakamoto, H. and Inoue, K. (2015). Interaction and colocalization of HERMES/RBPMS with NonO, PSF, and G3BP1 in neuronal cytoplasmic RNP granules in mouse retinal line cells. *Genes Cells* **20**, 257-266. doi:10.1111/gtc.12224

Gannon, H. S., Zou, T., Kiessling, M. K., Gao, G. F., Cai, D., Choi, P. S., Ivan, A. P., Buchumenski, I., Berger, A. C., Goldstein, J. T. et al. (2018). Identification of ADAR1 adenosine deaminase dependency in a subset of cancer cells. *Nat. Commun.* **9**, 5450. doi:10.1038/s41467-018-07824-4

Guillén-Boixet, J., Kopach, A., Holehouse, A. S., Wittmann, S., Jahnel, M., Schlüßler, R., Kim, K., Trussina, I. R. E. A., Wang, J., Mateju, D. et al. (2020). RNA-Induced Conformational Switching and Clustering of G3BP Drive Stress Granule Assembly by Condensation. *Cell.* **181**, 346-361.e17. doi:10.1016/j.cell.2020.03.049

Ha, S. C., Lokanath, N. K., Van Quyen, D., Wu, C. A., Lowenhaupt, K., Rich, A., Kim, Y. G. and Kim, K. K. (2004). A poxvirus protein forms a complex with left-handed Z-DNA: Crystal structure of a Yatapoxvirus Zα bound to DNA. *Proc. Natl. Acad. Sci. USA* **101**, 14367-14372. doi:10.1073/pnas.0405586101

Herbert, A. G. and Rich, A. (1993). A method to identify and characterize Z-DNA binding proteins using a linear oligodeoxynucleotide. *Nucleic Acids Res.* **21**, 2669-2672. doi:10.1093/nar/21.11.2669

Herbert, A., Alfken, J., Kim, Y. G., Mian, I. S., Nishikura, K. and Rich, A. (1997). A Z-DNA binding domain present in the human editing enzyme, double-stranded RNA adenosine deaminase. *Proc. Natl. Acad. Sci. USA* **94**, 8421-8426. doi:10.1073/pnas.94.16.8421

Kaiser, W. J., Upton, J. W. and Mocarski, E. S. (2008). Receptor-interacting protein homotypic interaction motif-dependent control of NF-kappa B activation via the DNA-dependent activator of IFN regulatory factors. *J. Immunol.* **181**, 6427-6434. doi:10.4049/jimmunol.181.9.6427

Ke, Y., Dramiga, J., Schütz, U., Kril, J. J., Ittner, L. M., Schröder, H. and Götz, J. (2012). Tau-mediated nuclear depletion and cytoplasmic accumulation of SFPQ in Alzheimer's and Pick's disease. *PLoS One* **7**, e35678. doi:10.1371/journal.pone.0035678

Kedersha, N., Chen, S., Gilks, N., Li, W., Miller, I. J., Stahl, J. and Anderson, P. (2002). Evidence that ternary complex (eIF2-GTP-tRNAiMet)-Deficient preinitiation complexes are core constituents of mammalian stress granules. *Mol. Biol. Cell* **13**, 195-210. doi:10.1091/mbc.01-05-0221

Kim, Y.-G., Muralinath, M., Brandt, T., Pearcy, M., Hauns, K., Lowenhaupt, K., Jacobs, B. L. and Rich, A. (2003). A role for Z-DNA binding in vaccinia virus pathogenesis. *Proc. Natl. Acad. Sci. USA* **100**, 6974-6979. doi:10.1073/pnas.0431131100

Kim, Y.-G., Lowenhaupt, K., Oh, D.-B., Kim, K. K. and Rich, A. (2004). Evidence that vaccinia virulence factor E3L binds to Z-DNA in vivo: Implications for development of a therapy for poxvirus infection. *Proc. Natl. Acad. Sci. USA* **101**, 1514-1518. doi:10.1073/pnas.0308260100

Kim, H.-E., Ahn, H.-C., Lee, Y.-M., Lee, E.-H., Seo, Y.-J., Kim, Y.-G., Kim, K. K., Choi, B.-S. and Lee, J.-H. (2011). The Zβ domain of human DAI binds to Z-DNA via a novel B-Z transition pathway. *FEBS Lett.* **585**, 772-778. doi:10.1016/j.febslet.2011.01.043

Kuś, K., Rakus, K., Boutier, M., Tsigkri, T., Gabriel, L., Vanderplasschen, A. and Athanasiadis, A. (2015). The Structure of the Cyprinid herpesvirus 3 ORF112-Zα·Z-DNA Complex Reveals a Mechanism of Nucleic Acids Recognition Conserved with E3L, a Poxvirus Inhibitor of Interferon Response. *J. Biol. Chem.* **290**, 30713-30725. doi:10.1074/jbc.M115.679407

Li, Y. (2011). The tandem affinity purification technology: An overview. *Biotechnol. Lett.* **33**, 1487-1499. doi:10.1007/s10529-011-0592-x

Li, H., Xiao, J., Li, J., Lu, L., Feng, S. and Dröge, P. (2009). Human genomic Z-DNA segments probed by the Zα domain of ADAR1. *Nucleic Acids Res.* **37**, 2737-2746. doi:10.1093/nar/gkp124

Li, Y. R., King, O. D., Shorter, J. and Gitler, A. D. (2013). Stress granules as crucibles of ALS pathogenesis. *J. Cell Biol.* **201**, 361-372. doi:10.1083/jcb.201302044

Loughlin, F. E., Lukavsky, P. J., Kazeeva, T., Reber, S., Hock, E. M., Colombo, M., Von Schroetter, C., Pauli, P., Cléry, A., Mühlemann, O. et al. (2019). The Solution Structure of FUS Bound to RNA Reveals a Bipartite Mode of RNA Recognition with Both Sequence and Shape Specificity. *Mol. Cell* **73**, 490-504.e6. doi:10.1016/j.molcel.2018.11.012

Lu, L., Han, A.-P. and Chen, J.-J. (2001). Translation Initiation Control by Heme-Regulated Eukaryotic Initiation Factor 2α Kinase in Erythroid Cells under Cytoplasmic Stresses. *Mol. Cell. Biol.* **21**, 7971-7980. doi:10.1128/MCB.21.23.7971-7980.2001

Masuda, A., Takeda, J. I., Okuno, T., Okamoto, T., Ohkawara, B., Ito, M., Ishigaki, S., Sobue, G. and Ohno, K. (2015). Position-specific binding of FUS to nascent RNA regulates mRNA length. *Genes Dev.* **29**, 1045-1057. doi:10.1101/gad.255737.114

Masuda, A., Takeda, Ichi, J. and Ohno, K. (2016). FUS-mediated regulation of alternative RNA processing in neurons: Insights from global transcriptome analysis. *Wiley Interdiscip. Rev. RNA* **7**, 330-340. doi:10.1002/wrna.1338

Mellacheruvu, D., Wright, Z., Couzens, A. L., Lambert, J. P., St-Denis, N. A., Li, T., Miteva, Y. V., Hauri, S., Sardiu, M. E., Low, T. Y. et al. (2013). The CRAPome: A contaminant repository for affinity purification-mass spectrometry data. *Nat. Methods* **10**, 730-736. doi:10.1038/nmeth.2557

Morgenstern, J. P. and Land, H. (1990). Advanced mammalian gene transfer: High titre retroviral vectors with multiple drug selection markers and a complementary

helper-free packaging cell line. *Nucleic Acids Res.* **18**, 3587-3596. doi:10.1093/nar/18.12.3587

Ng, S. K., Weissbach, R., Ronson, G. E. and Scadden, A. D. J. (2013). Proteins that contain a functional Z-DNA-binding domain localize to cytoplasmic stress granules. *Nucleic Acids Res.* **41**, 9786-9799. doi:10.1093/nar/gkt750

Oh, D.-B., Kim, Y.-G. and Rich, A. (2002). Z-DNA-binding proteins can act as potent effectors of gene expression in vivo. *Proc. Natl. Acad. Sci. USA* **99**, 16666-16671. doi:10.1073/pnas.262672699

Passon, D. M., Lee, M., Rackham, O., Stanley, W. A., Sadowska, A., Filipovska, A., Fox, A. H. and Bond, C. S. (2012). Structure of the heterodimer of human NONO and paraspeckle protein component 1 and analysis of its role in subnuclear body formation. *Proc. Natl. Acad. Sci. USA* **109**, 4846-4850. doi:10.1073/pnas.1120792109

Peng, P. L., Zhong, X., Tu, W., Soundarapandian, M. M., Molner, P., Zhu, D., Lau, L., Liu, S., Liu, F. and Lu, Y. M. (2006). ADAR2-dependent RNA editing of AMPA receptor subunit GluR2 determines vulnerability of neurons in forebrain ischemia. *Neuron* **49**, 719-733. doi:10.1016/j.neuron.2006.01.025

Pérez-González, A., Pazo, A., Navajas, R., Ciordia, S., Rodriguez-Frandsen, A. and Nieto, A. (2014). HCLE/C14orf166 associates with DDX1-HSPC117-FAM98B in a novel transcription-dependent shuttling RNATransporting complex. *PLoS One* **9**, e90957. doi:10.1371/journal.pone.0090957

Perrot, I., Deauvieau, F., Massacrier, C., Hughes, N., Garrone, P., Durand, I., Demaria, O., Viaud, N., Gauthier, L., Blery, M. et al. (2010). TLR3 and Rig-Like Receptor on Myeloid Dendritic Cells and Rig-Like Receptor on Human NK Cells Are Both Mandatory for Production of IFN-γ in Response to Double-Stranded RNA. *J. Immunol.* **185**, 2080-2088. doi:10.4049/jimmunol.1000532

Placido, D., Brown, B. A., Lowenhaupt, K., Rich, A. and Athanasiadis, A. (2007). A Left-Handed RNA Double Helix Bound by the Zα Domain of the RNA-Editing Enzyme ADAR1. *Structure* **15**, 395-404. doi:10.1016/j.str.2007.03.001

Prasanth, K. V., Prasanth, S. G., Xuan, Z., Hearn, S., Freier, S. M., Bennett, C. F., Zhang, M. Q. and Spector, D. L. (2005). Regulating gene expression through RNA nuclear retention. *Cell* **123**, 249-263. doi:10.1016/j.cell.2005.08.033

Rice, G. I., Kasher, P. R., Forte, G. M. A., Mannion, N. M., Greenwood, S. M., Szynkiewicz, M., Dickerson, J. E., Bhaskar, S. S., Zampini, M., Briggs, T. A. et al. (2012). Mutations in ADAR1 cause Aicardi-Goutières syndrome associated with a type i interferon signature. *Nat. Genet.* **44**, 1243-1248. doi:10.1038/ng.2414

Rothenburg, S., Deigendesch, N., Dittmar, K., Koch-Nolte, F., Haag, F., Lowenhaupt, K. and Rich, A. (2005). A PKR-like eukaryotic initiation factor 2α kinase from zebrafish contains Z-DNA binding domains instead of dsRNA binding domains. *Proc. Natl. Acad. Sci. USA* **102**, 1602-1607. doi:10.1073/pnas.0408714102

Scadden, A. D. J. (2005). The RISC subunit Tudor-SN binds to hyper-edited double-stranded RNA and promotes its cleavage. *Nat. Struct. Mol. Biol.* **12**, 489-496. doi:10.1038/nsmb936

Scadden, A. D. J. (2007). Inosine-Containing dsRNA Binds a Stress-Granule-like Complex and Downregulates Gene Expression In trans. *Mol. Cell* **28**, 491-500. doi:10.1016/j.molcel.2007.09.005

Schwartz, T., Rould, M. A., Lowenhaupt, K., Herbert, A. and Rich, A. (1999). Crystal structure of the Zα domain of the human editing enzyme ADAR1 bound to left-handed Z-DNA. *Science* **284**, 1841-1845. doi:10.1126/science.284.5421.1841

Schwartz, T., Behlke, J., Lowenhaupt, K., Heinemann, U. and Rich, A. (2001). Structure of the DLM-1-Z-DNA complex reveals a conserved family of Z-DNA-binding proteins. *Nat. Struct. Biol.* **8**, 761-765. doi:10.1038/nsb0901-761

Sharathchandra, A., Lal, R., Khan, D. and Das, S. (2012). Annexin A2 and PSF proteins interact with p53 IRES and regulate translation of p53 mRNA. *RNA Biol.* **9**, 1429-1439. doi:10.4161/rna.22707

Shelkovnikova, T. A., Robinson, H. K., Troakes, C., Ninkina, N. and Buchman, V. L. (2014). Compromised paraspeckle formation as a pathogenic factor in FUSopathies. *Hum. Mol. Genet.* **23**, 2298-2312. doi:10.1093/hmg/ddt622

Sung, C. H., Kim, D., Hwang, H.-Y., Rich, A., Kim, Y.-G. and Kyeong, K. K. (2008). The crystal structure of the second Z-DNA binding domain of human DAI (ZBP1) in complex with Z-DNA reveals an unusual binding mode to Z-DNA. *Proc. Natl. Acad. Sci. USA* **105**, 20671-20676. doi:10.1073/pnas.0810463106

Takaoka, A., Wang, Z., Choi, M. K., Yanai, H., Negishi, H., Ban, T., Lu, Y., Miyagishi, M., Kodama, T., Honda, K. et al. (2007). DAI (DLM-1/ZBP1) is a cytosolic DNA sensor and an activator of innate immune response. *Nature* **448**, 501-505. doi:10.1038/nature06013

Tourrière, H., Chebli, K., Zekri, L., Courselaud, B., Blanchard, J. M., Bertrand, E. and Tazi, J. (2003). The RasGAP-associated endoribonuclease G3BP assembles stress granules. *J. Cell Biol.* **160**, 823-831. doi:10.1083/jcb.200212128

Vitali, P. and Scadden, A. D. J. (2010). Double-stranded RNAs containing multiple IU pairs are sufficient to suppress interferon induction and apoptosis. *Nat. Struct. Mol. Biol.* **17**, 1043-1050. doi:10.1038/nsmb.1864

Wang, X., Schwartz, J. C. and Cech, T. R. (2015). Nucleic acid-binding specificity of human FUS protein. *Nucleic Acids Res.* **43**, 7535-7543. doi:10.1093/nar/gkv679

Weissbach, R. and Scadden, A. D. J. (2012). Tudor-SN and ADAR1 are components of cytoplasmic stress granules. *RNA* **18**, 462-471. doi:10.1261/rna.027656.111

Yang, J., Välineva, T., Hong, J., Bu, T., Yao, Z., Jensen, O. N., Frilander, M. J. and Silvennoinen, O. (2007). Transcriptional co-activator protein p100 interacts with snRNP proteins and facilitates the assembly of the spliceosome. *Nucleic Acids Res.* **35**, 4485-4494. doi:10.1093/nar/gkm470

Yarosh, C. A., Iacona, J. R., Lutz, C. S. and Lynch, K. W. (2015). PSF: Nuclear busy-body or nuclear facilitator? *Wiley Interdiscip. Rev. RNA* **6**, 351-367. doi:10.1002/wrna.1280

Zhang, Z. and Carmichael, G. G. (2001). The fate of dsRNA in the nucleus: a p54(nrb)-containing complex mediates the nuclear retention of promiscuously A-to-I edited RNAs. *Cell* **106**, 465-475. doi:10.1016/s0092-8674(01)00466-4